# Laminar - turbulent transition in the propagation of height-contained hydraulic fracture

Zia, H. and Lecampion, B.
*Geo-Energy Lab - Gaznat chair on Geo-Energy, ENAC-IIC-GEL, EPFL, Switzerland*

**ABSTRACT:** High injection rate hydraulic fracturing can have Reynolds number as high as $10^4$. For such high Reynolds numbers, turbulent flow is likely to occur. In this paper, we investigate the effect of turbulence on the propagation of hight contained hydraulic fractures, commonly referred to as PKN fractures. We discuss different scalings for the fracture width, length and pressure under limiting laminar, turbulent smooth and turbulent rough flow regimes. We implement an explicit, central numerical scheme to solve the continuity and friction factor based momentum conservation equations, taking into account the full variation of friction factor with Reynolds number and relative fracture roughness. The scheme is validated against the analytical solution of the PKN model. The results show that the local Reynolds number evolves from a maximum value at the inlet to zero at the tip, with a transition from turbulent to laminar at some point along the fracture length, depending on the value of inlet Reynolds number. Results showing the effect of smooth and rough turbulence on the fracture length and fracture width depending on the Reynolds number are finaly presented.

## 1 Introduction

The usual approximation of laminar flow in a propagating hydraulic fracture sometimes breakdown. This is the case of fluid-driven fracture propagation at glacier beds where Reynolds numbers above $10^5$ are expected (Tsai and Rice (2010)). At such large Reynolds numbers, the flow is well within the turbulent rough regime. Recently, Ames and Bunger (2015) have investigated the effect of a fully rough turbulent flow on the propagation of height contained hydraulic fracture (Nordgren (1972)) and derived scaling relationship for that flow regime. However, in practice for a hydraulic fracture treatment in an oil and gas reservoir using a low viscosity fluid injected at very large injection rate, the Reynolds number for a height contained fracture are expected to be in the range $10^3 - 10^4$ at most (see Table 1 and 2), right in the transition between the laminar to the fully turbulent regime. We focus solely here on a height contained fracture as depicted in Fig. 1 (i.e. the so-called PKN geometry). In parallel to the problem formulation, we also review the available experimental data and models covering the complete flow conditions spanning the complete spectrum of Reynolds numbers from laminar to fully turbulent. We notably discuss the use of an equivalent Reynolds number proposed by Jones (1976) to use the available data and models developed for flow in pipes to the case of elliptical cross-section encountered in the PKN geometry.

We then present a numerical model for the propagation of a height contained hydraulic fracture (PKN fractures) accounting for the complete laminar - turbulent transition . Our algorithm is based on a non-diffusive central scheme with fixed grid and explicit time-stepping. We fully validate our scheme against the well-known laminar case (Nord-

| Parameter | Value |
|-----------|-------|
| $\rho$ | $1000\mathrm{kg/m^3}$ |
| $\mu$ | $8 \times 10^{-4}\mathrm{Pa\,s}$ |
| $h$ | 10m |
| $E'$ | 32 GPa |
| $k$ | 1 mm |

Table 1: Typical values of rock, fluid properties and fracture height $h$. $k$ denotes a fracture roughness lengthscale.

| $Q_0$ (bbl/min) | $Q_0$ (m³/s) | $\mathcal{R} = \dfrac{Q_o\rho}{2h\mu}$ |
|-----------------|--------------|-----------------------------------------|
| 10 | 0.026 | 650 |
| 20 | 0.053 | 1325 |
| 30 | 0.079 | 1975 |
| 40 | 0.106 | 2650 |

Table 2: Inlet Reynolds number ($\mathcal{R}$) in a height contained fractures for different values of injection rate and evaluated with the parameters listed in Table 1 for density, viscosity and fracture height. Transition to turbulent flow starts at $\mathcal{R}_c \approx 1380$ for such geometry.

gren (1972)). We finally discuss the relevance of the different limiting approximations (i.e. fully laminar versus fully turbulent regime) to simulate typical industrial hydraulic fracturing treatments in unconventional reservoirs.

# 2 Problem formulation

We consider a height contained bi-wing hydraulic fracture of half-length $\ell$ propagating in the $x$-direction, with a width of $w(x, z)$ (see Figure 1). The fracture is assumed to be bounded by two layers of highly stressed rocks at the top and bottom of the reservoir, restricting its height to $h$ vertically. The rock layer is assumed to be linear-elastic with a plane strain Young's modulus $E'$. The fracture is driven by the injection of a Newtonian fluid of viscosity $\mu$ and density $\rho$ at a constant flow rate $Q_o$. The fracture length is assumed to be much larger than its height and the fluid flow is assumed to be uni-dimensional in the direction of propagation.
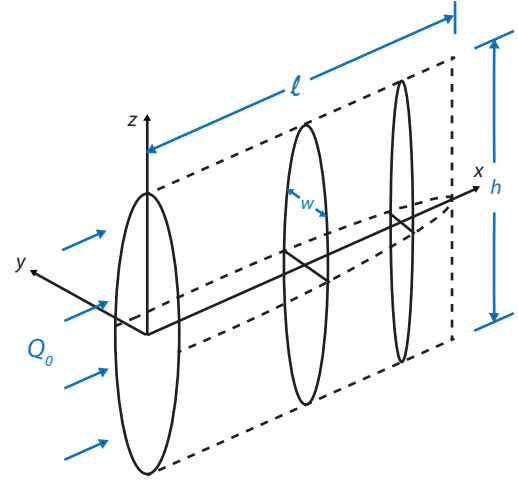


Figure 1: Sketch of a height-contained hydraulic fracture (PKN geometry e.g. Economides and Nolte (2000)).

## 2.1 Elasticity

The length of the fracture is assumed to be sufficiently large compared to its height such that every vertical cross-section can be assumed to be in a state of plane-strain. Following the approximation of uni-directional flow, the net pressure $p(x)$, which is equal to the excess of the fluid pressure above the compressive in-situ stress is assumed to be uniform in each vertical cross-section. As a result, the plain strain elasticity solution for an uniformly pressurized fracture provides the following local relation between the fracture width $w(x, z)$ and the net pressure $p(x)$ at a given cross-section located at $x$ (e.g. Sneddon and Elliot (1946)):

$$w(x, z) = \frac{2hp(x)}{E'}\sqrt{1 - \frac{4z^2}{h^2}}, \qquad (1)$$

where $E' = E/(1 - \nu^2)$ is the plane-strain modulus. By defining $\overline{w}$ as the average fracture width given by $\frac{1}{h}\int_{-h/2}^{h/2} w(x, z)dz$, Eq. (1) gives (e.g. Sarvaramini and Garagash (2015)):

$$\bar{w}(x) = \frac{\pi}{4}\frac{2hp(x)}{E'} = \frac{\pi}{4}w(x, 0).$$

## 2.2 Continuity

Neglecting fluid compressibility, the local fluid mass conservation reduces to the following continuity equation:

$$\frac{\partial A}{\partial t} + \frac{\partial Q}{\partial x} = 0, \qquad (2)$$

where $A = \overline{w}h$ is the cross-sectional area of the fracture in the $y$-$z$ plane, $Q = A\overline{v}$ is the volumetric flow rate of the fluid and $\overline{v}$ is the cross-sectional average of the fluid velocity in the $x$-direction. The rock is assumed be impermeable and fluid leak off from the fracture faces is thus neglected.

## 2.3 Boundary conditions

The fluid is injected at $x = 0$ into the bi-wing fracture at a flow rate $Q_0$. The flow rate entering one wing of the fracture is thus:

$$Q(x = 0) = \frac{Q_0}{2} \qquad (3)$$

The boundary conditions at the fracture tip $(x = \ell)$ are given by:

$$Q(x = \ell) = 0 \qquad \overline{w}(x = \ell) = 0 \qquad (4)$$

## 2.4 Momentum Conservation

The cross-sectional average of the fluid momentum conservation equation reduces to:

$$\rho\left(\frac{\partial Q}{\partial t} + \frac{\partial Q\overline{v}}{\partial x}\right) = -A\frac{\partial p}{\partial x} - Þ\tau_w, \qquad (5)$$

where Þ is the perimeter of the cross-section of the fracture and $\tau_w$ is the wall shear stress given by

$$\tau_w = f\frac{\rho\overline{v}^2}{2}.$$

Here, $f$ is the Fanning friction factor which is a function of the local value of the Reynolds number as well as the relative roughness of the fracture in the turbulent regime.

### 2.4.1 Friction Factor

To solve the set of equations (1)-(5), the dependence of the friction factor on the Reynolds number and the relative roughness must be estimated. The classical experiments of Nikuradse (1950) have provided the basis for a number of empirical relations between the Reynolds number and the friction factor in smooth and rough pipes. These relations cannot be directly applied to the case of fluid flow in a fracture, especially one having an elliptical cross-section. The concept of hydraulic diameter provides a method to accommodate different channel geometries but experimental studies have demonstrated that the obtained relations are not accurate (Sadatomi, Sato and Saruwatari, 1982; Carlson and Irvine, 1961; Jones, 1976). Jones (1976) introduced the concept of a "laminar equivalent" hydraulic diameter in order to obtain the friction factor for rectangular cross-sections using the friction factor vs. Reynolds number relation for circular cross-sections. This laminar equivalent hydraulic diameter is obtained such that the friction factor can be expressed using the same expression as for the laminar flow in circular pipes (i.e. the analytically obtained expression $f_L = 16/Re$).

The laminar equivalent hydraulic diameter for an elliptical cross-section can be obtained by comparing the solution of a pressure-driven flow in elliptical geometry (see e.g. Lamb (1895)) to the solution calculated by the friction factor based wall-shear stress in laminar conditions. By introducing $\alpha$ as a geometry-dependent coefficient necessary to get the correct equivalence between the two solutions, the "pipe-equivalent" Reynolds number is evaluated as $\alpha D_H \frac{\overline{v}\rho}{\mu}$, where $D_H = 4A/Þ$ is the hydraulic diameter. For an ellipse with a very large major axis compared to the minor one, as is the case with fractures, $\alpha = 25/32$ gives the correct equivalence. The "pipe-equivalent" Reynolds number $(\overline{Re})$ for the PKN elliptical cross-section is thus:

$$\overline{Re} = \alpha 4\frac{A}{Þ}\frac{\rho\overline{v}}{\mu} = \frac{32}{5\pi}\frac{\overline{w}\alpha\rho\overline{v}}{\mu} = \frac{5}{\pi}\frac{\rho\overline{w}\overline{v}}{\mu} = \frac{5}{\pi}Re.$$

where $Re = \dfrac{\rho\overline{w}\overline{v}}{\mu}$ is the Reynolds computed using simply the averaged fracture width as the flow di-

mension. Using this pipe-equivalent Reynolds number, the friction factor can be evaluated with the relations for a circular cross-section, i.e. $f_L = 16/\overline{Re}$ in the laminar flow regime. In the turbulent regime, we use the relations of Blasius and Manning-Strickler for fully smooth and fully rough flows respectively:

$$f_B = f'_B \, \overline{Re}^{-1/4} \qquad f'_B = 0.316/4$$

$$f_M = f'_M \left(\frac{k}{\overline{w}}\right)^{1/3} \qquad f'_M = 0.143/4$$

where $k$ denotes the roughness lengthscale, $f'_B$ and $f'_M$ are the coefficients appearing in the Blasius and Manning-Strickler relations respectively. The transition from the laminar to the different turbulent regimes is mapped using an approximation recently proposed by Yang and Dou (2010). It is an implicit function which can be used to calculate the friction factor, given the Reynolds number and relative roughness of the pipe. The complete evolution of the friction factor with the Reynolds number and relative roughness $(k/D)$ obtained in pipe flow experiments by Nikuradse Nikuradse (1950) is shown in Figure 2. Different approximations used in this study are also shown. Note that the critical Reynolds number at which turbulence starts is about 2200 for circular pipes. The critical value for an elliptical cross-section is thus $Re_c = 2300 \times \pi/5 \approx 1380$.

# 3 Dimensional analysis and scaling

Using the following scaled coordinates system

$$\xi = x/\ell(t)$$

where $\ell(t)$ is the length of the fracture at a given time, and introducing the following characteristic scales (possibly function of time):

$$W_*, \ P_*, \ V_*, \ L_*,$$

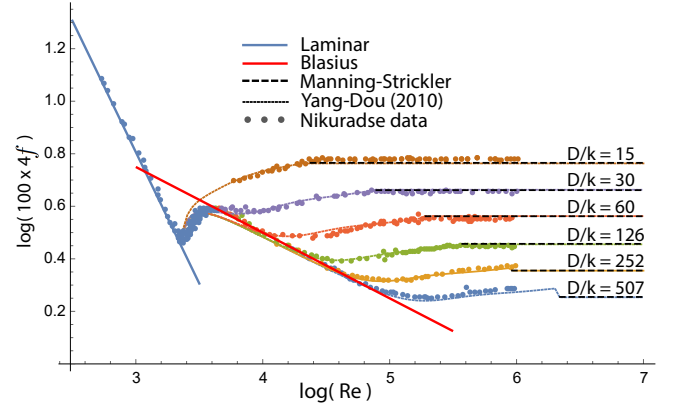

Figure 2: Nikuradse (1950) data: friction factor as function of the Reynolds number ($Re = \rho v D/\mu$) and relative roughness in pipes. The laminar, Blasius, Manning-Strickler and Yang-Dou approximations are also shown.

it is possible to show that the inertial terms in the balance of momentum have always a negligible effect for time larger than $\sqrt{\mathcal{R} \times \frac{W_*}{L_*}}$ (a time-scale which is always negligible due to the fact that the characteristic width is always much smaller than the fracture characteristic length). Here, $\mathcal{R}$ denotes the value of the Reynolds number $\mathcal{R} = \frac{\rho W_* V_*}{\mu} = \frac{1}{2}\frac{Q_o \rho}{h\mu}$ at the fracture inlet. Assuming laminar friction, one recovers the scaling of the classical PKN solution - which we indicate with a subscript $L$ for laminar:

$$W_L = \left(\frac{\mu \pi^3 Q_0^2 t}{2^3 E' h}\right)^{1/5} \qquad L_L = \left(\frac{E' Q_0^3 t^4}{2^2 h^4 \mu \pi^3}\right)^{1/5}$$

$$P_L = \frac{2 W_L E'}{h\pi} \qquad V_L = L_L/t.$$

As discussed in Ames and Bunger (2015), assuming a purely turbulent rough regime governed by Manning-Strickler friction over the whole fracture, we obtain the following "fully-rough" scaling, indicated with a subscript $R$:

$$W_R = \frac{5^{3/16} f'^{3/16}_M k^{1/16} \pi^{3/8} Q_0^{9/16} \rho^{3/16} t^{3/16}}{2\sqrt{2} E'^{3/16} h^{3/8}}$$

$$L_R = \frac{\sqrt{2} E'^{3/16} Q_0^{7/16} t^{13/16}}{5^{3/16} f'^{3/16}_M h^{5/8} k^{1/16} \pi^{3/8} \rho^{3/16}}$$

$$P_R = \frac{2W_R E'}{h\pi} \qquad V_R = L_R/t.$$

Similarly, assuming a purely turbulent but smooth flow regime where friction is governed by Blasius relation, we obtain the following characteristic scales for "fully-smooth" turbulent scaling, indicated with a subscript $S$:

$$W_S = \frac{5^{3/20}\pi^{9/20}}{2 \times 2^{11/20}} \frac{f_B'^{1/5}\mu^{1/20}Q_o^{11/20}\rho^{3/20}t^{1/5}}{E'^{1/5}h^{7/20}}$$

$$L_S = \frac{2^{11/20}}{5^{3/20}\pi^{9/20}} \frac{E'^{1/5}Q_o^{9/20}t^{4/5}}{f_B'^{1/5}h^{13/20}\mu^{1/20}\rho^{3/20}}$$

$$p_S = \frac{2W_B E'}{h\pi} \qquad V_S = L_S/t$$

In these limiting regimes (laminar, fully turbulent rough and fully turbulent smooth), the propagation of the hydraulic fracture can actually shown to be self-similar. The complete dimensionless solutions can be obtained semi-analytically in a similar way as for the classical PKN solution. Details are omitted here for brevity. For example, the fracture length assuming complete turbulent rough flow is given by $\ell_R(t) = 1.08L_R(t)$, while for the fully turbulent smooth-Blasius regime $\ell_S(t) = 1.09L_S(t)$ and the classical laminar solution for fracture length is $\ell_L(t) = 1.001L_L(t)$. Similarly, $w_R(x,t) = W_R(t)\Omega_R(\xi)$, $w_S(x,t) = W_S(t)\Omega_S(\xi)$ and $w_L(x,t) = W_L(t)\Omega_L(\xi)$ gives the fracture width for laminar, turbulent smooth and turbulent rough flows respectively, where $\Omega$ is the dimensionless opening of order 1.

In reality, the value of friction varies spatially with the local value of the Reynolds number ($Re = \mathcal{R}\Psi$), which depends on the local value of the dimensionless flow rate $\Psi = \Omega \times \Upsilon$ (where $\Upsilon$ is the dimensionless velocity). The dimensionless flow rate has the value of 1 at the fracture inlet and is equal to zero at the fracture tip according to the boundary conditions (3)-(4). We therefore see that inevitably, the flow will always be in the laminar regime at the fracture tip, potentially shrinking to

a laminar boundary layer at the fracture tip, if the flow is highly turbulent at the fracture inlet. In order to investigate the complete transition of the flow regime from laminar to turbulent, a numerical solution thus is necessary using the complete transition of the friction factor from the laminar to the turbulent regime (smooth or rough).

Another interesting point worth mentioning here relates to the slightly different power-law of time dependence obtained for the fully rough regime (as already mentioned by Ames and Bunger (2015)). In the case where the complete transition is accounted for inside the fracture, one can intuitively grasp that if turbulent, the flow will be first turbulent rough as the fracture opening will be of the order of the roughness lengthscale $k$ at early time. As the fracture grows and the width increases, the flow can eventually transition to the turbulent smooth regime. The time-scale of the transition from the rough to the smooth turbulent regime can be estimated as:

$$t_{R\to S} = \frac{16E'k^5\rho^3 Q_o}{5\pi^2 f_M'h^2\mu^4},$$

a time-scales obtained from the fact that roughness has negligible effect on friction when $\left(\dfrac{k}{W_R}\right)\mathcal{R}^{3/4} \approx 1$ and friction tends to the Blasius limit (Goldenfeld, 2006). It is interesting to note that using realistic values for a slickwater treatment (e.g. shown in Table 1) and for an injection rate of 0.026m³/s (10bbl/min), we obtain $t_{R\to S} \approx 2\times10^{13}$sec, indicating that if turbulent, the flow will never reach the limiting regime of turbulent smooth / Blasius type flow in practice.

# 4 Numerical Scheme & validation

We solve the system of equations (1)-(5) with a second, order non-oscillatory central scheme introduced by Nessyahu and Tadmor (1990). Such an explicit scheme operates in a predictor-corrector fashion. To ensure numerical stability, the scheme upholds TVD (total variation diminishing) property by using slope and flux limiters. An impor-

tant characteristic of the scheme is that it does not utilize any Riemann-solver, which makes it easy to implement. The Riemann-solver free formulation is made possible by the use of staggered grids, allowing integration over the entire Riemann fan and taking into account both the left and right-going waves (see Nessyahu and Tadmor (1990) for details). A well-known factor limiting the use of central scheme is that it can become highly diffusive (see e.g. Kurganov and Tadmor (2000); Kurganov and Lin (2007)), especially for highly non-linear problems such as the one under consideration here. In this study, we use an anti-diffusive correction introduced recently by Zia and Simpson (under-review) that allows the diffusion to be mitigated with the cost of a smaller CFL bound on the time step.

To demonstrate the accuracy of the scheme, the system is solved using only the laminar expression for the friction factor : $f_L = 16/\overline{Re}$. In this case, the model is strictly equivalent to the classical PKN hydraulic fracture model, for which an analytical solution is available (Nordgren (1972)). The numerical solution is obtained by discretizing the domain with a fixed Cartesian mesh of 150 cells. A re-meshing is performed as soon as the fracture tip reaches the end of the computational domain. Correct location of the fracture tip is important as the solution is sensitive to its position and even a small diffusion can introduce significant error. We are characterizing fracture to be open at the point along the length of the fracture where the opening goes above a small value (taken here as $2 \times 10^{-5}$m). The fracture is assumed to be propagating with a fixed velocity inside a cell, which is evaluated each time the tip moves to the next cell. To mitigate numerical diffusion, a large value of 0.999 is used for the correction factor $\epsilon$ (see Zia (2015) for description of this correction parameter) to solve the continuity equation. Use of this high correction factor allows to significantly decrease the numerical diffusion but as a drawback, it can introduce spurious oscillations in the solution. A small Courant number of 0.015 is thus imposed to calculate the time step, ensuring the numerical stability of the scheme. The parameters used for this benchmark are the one listed in Table 1 with an injection rate of $Q_0 = 0.03$ m$^3$/s. Initial conditions are prescribed as the exact laminar solutions ($w_0(x) = w_L(x, t_0)$and $\ell_0 = \ell_L(t_0)$) at a given initial time $t_0$ (2 sec in this test case) .

The numerical results are shown in Figures 3-5 over close to four decades of time. Figure 3 shows the evolution of the scaled fracture-length $\ell(t)/\ell_0$ vs scaled time $(t/t_0)$ and the scaled fracture-width at the inlet $w(0, t)/w_0$ vs scaled time $(t/t_0)$ on the bottom and top respectively. A very good match with the analytical solutions can be observed. Furthermore, the relative error of the fracture-length and the fracture-width are shown in Figure 4 on the bottom and top respectively. The sharp jumps in the time evolution of error are due to re-meshing which is performed as the fracture tip reaches the end of the computational domain. The remeshing introduces a small error due to loss of data caused by interpolations, which does not fully recovers before the next remeshing step resulting in accumulation of a small error as the solution evolves. The results show that this error accumulation is not significant: the relative error does not exceeds 0.3 and 2 percent for the fracture width and fracture length respectively over close to four decades of time which is more than enough for practical cases. The fracture width shown in Figure 3 is the width at the fluid inlet. Figure 5 shows the profile of the dimensionless fracture width at different values of the scaled time $(\tau = t/t_0)$ along with the analytical solution. It can be seen that the numerical solution matches the analytical solution very well, apart from the small diffusion at the fracture tip which does not appear to "grow" in time.

# 5 Results

The inlet value of the Reynolds number $\mathcal{R}$ directly provides information about the flow regime when compared to the empirically known critical value ($\approx 1380$ for a fracture with elliptical cross-section as mentioned previously), above which the flow becomes turbulent. To evaluate the effect of turbulence on the propagation of the fracture, we have performed a number of numerical simulations discussed below.
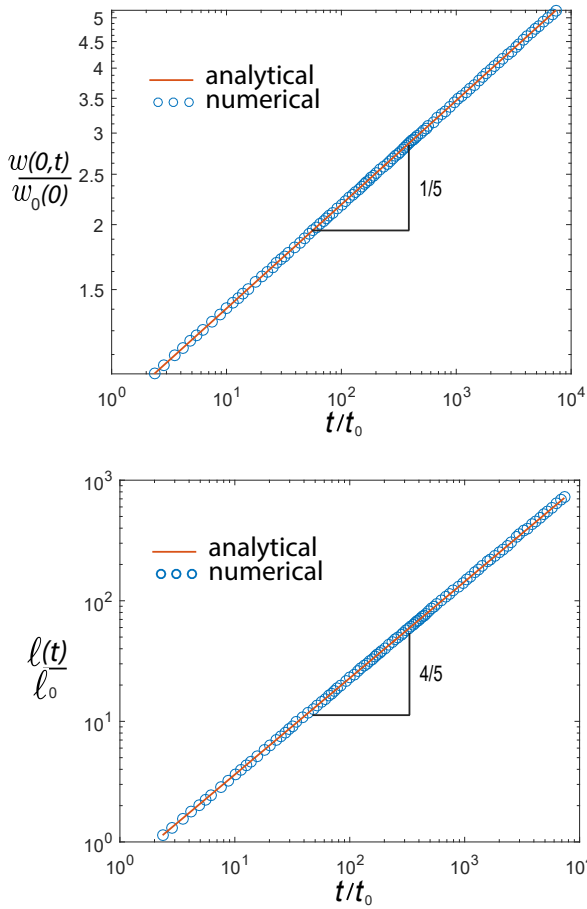
Figure 3: Fully Laminar Case ($f = f_L$): Evolution with scaled time of the scaled fracture length (bottom) and scaled fracture width at the fracture inlet (top).
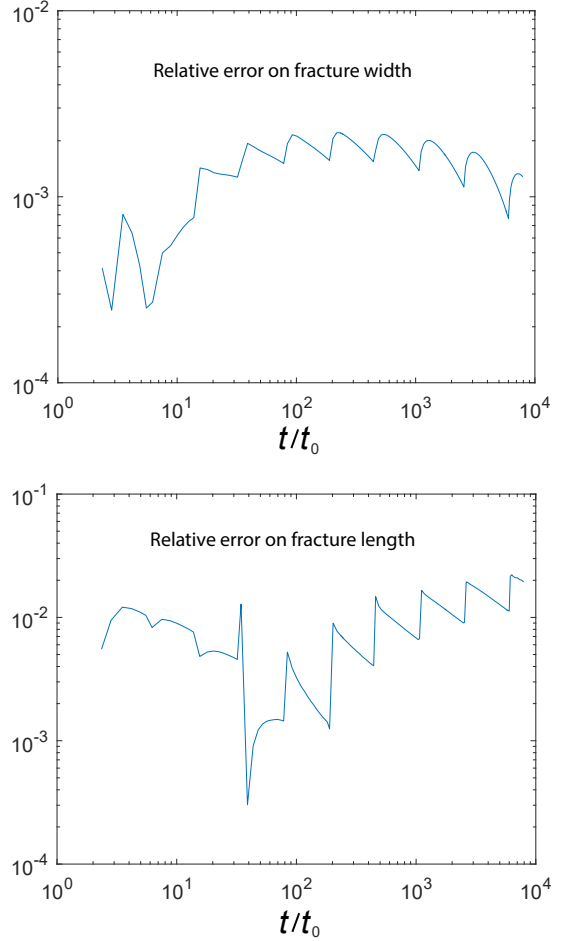


Figure 4: Fully Laminar Case ($f = f_L$): Evolution with scaled time of the Relative error of the numerical solution for fracture-length (bottom) and fracture-width (top).

## 5.1 Smooth fracture case

We first discuss the results for the case where the effect of fracture roughness is neglected: i.e. assuming a transition from laminar to Blasius like turbulent flow to compute the friction factor (see Figure 2). We have performed a set of simulations for different values of $\mathcal{R}$ to determine the relative position ($\xi_t$) of the laminar to turbulent transition along the fracture. The simulations were performed with a grid of 150 cells. Figure 6 shows the relative size of the laminar region against different values of $\mathcal{R}$. It can be seen that the relative size of the laminar region $1 - \xi_t$ is of the value 1, indicating the whole fracture is in laminar regime for the values of $\mathcal{R}$ below the critical value. The size decreases

as the Reynolds number increases above the critical value until the size of the laminar layer falls below the spatial resolution of the simulation, i.e. it cannot be resolved with any more precision than the scaled grid size $1/N = 1/150$, where $N$ is the number of element in the grid.

The fracture length and width for the same series of simulations are shown in Figure 7, top and bottom respectively. The results are shown relative to the semi-analytical laminar solutions (Nordgren, 1972). It can be seen that the relative fracture length has the value of one for the values of $\mathcal{R}$ below the critical value and it decreases as the value of $\mathcal{R}$ increases. Figure 7 also shows the ratio of the semi-analytical solutions ($w_S(0,t)/w_L(0,t)$ and
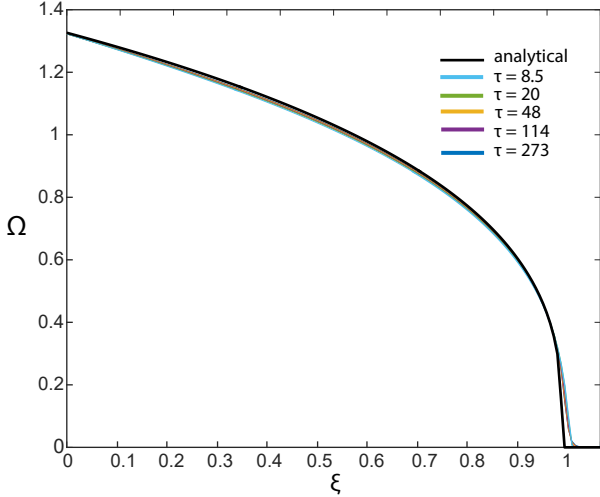
Figure 5: Fully Laminar Case ($f = f_L$): Analytical and numerical solutions for dimensionless fracture width. The small numerical diffusion observed at the fracture tip does not grow in time and is intrinsically related to the corrected adNOC scheme used here.



Figure 6: Laminar-Turbulent Smooth case: Relative length ($1 - \xi_t$) of the laminar fraction of the flow for different values of $\mathcal{R}$.

$\ell_S(t)/\ell_L(t)$. It can be seen that the slope of the numerical results is initially lower for Reynolds numbers where the size of the laminar boundary layer is still significant and finally converges to the analytical slope when the laminar boundary layer is so small that it becomes insignificant and the whole fracture can be assumed to be in turbulent smooth regime. Similar results for the fracture width evolution are also shown. The fact that our numerical scheme converges with the fully-smooth turbulent solution is another indication of its accuracy.

## 5.2 Including roughness

As discussed before, the scalings show that the regime is almost always turbulent rough due to very high $t_{R \to S}$ for realistic parameters. We have performed simulations with two different Reynolds numbers ($\mathcal{R}$) of $2.5 \times 10^3$ and $10^4$. In the case of $10^4$, the Reynolds number is well into the turbulent rough regime. In this case, the size of the laminar boundary layer is very small and the whole fracture can be assumed to be in fully turbulent rough regime. For Reynolds number
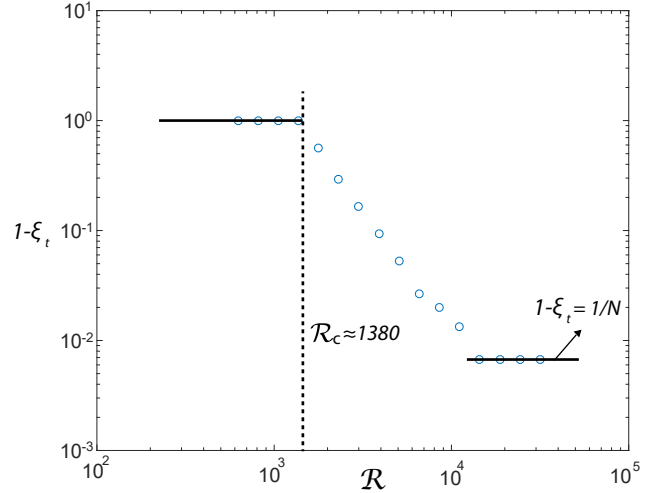
of 2500, the flow regime is always in the laminar to turbulent transition. The fracture width ($w(0, \tau)/w_L(0, \tau)$) and fracture length ($\ell(\tau)/\ell_L(\tau)$) relative to the laminar solutions against the dimensionless time ($\tau = t/t_{R \to S}$) for the two different Reynolds number are shown in Figure 8, top and bottom respectively. The laminar solutions are evaluated with the corresponding Reynolds number for both cases. The analytical turbulent rough solutions ($w_R(0, \tau)/w_L(0, \tau)$ and $\ell_R(\tau)/\ell_L(\tau)$) for both Reynolds numbers are also shown. It can be observed that the fracture solutions tends to the fully turbulent rough limit for the Reynolds number of $10^4$, indicating insignificant size of the laminar layer. For $\mathcal{R} = 2.5 \times 10^{-3}$, the fracture width is smaller than the limiting turbulent rough solution but larger than the limiting laminar solution, indicating that the flow regime lies in the laminar to rough transition.

## 6 Conclusions

We have investigated the effect of turbulent flow on the propagation of height contained hydraulic fractures. Using the concept of equivalent laminar hydraulic radius (Jones, 1976), we have used the
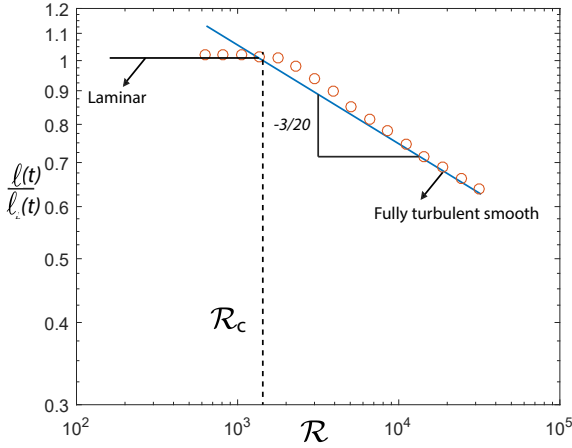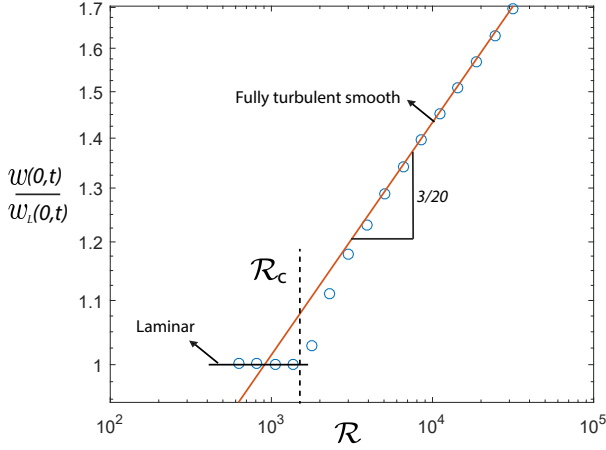
Figure 7: Laminar-Turbulent Smooth case: The fracture length (top) and fracture width (bottom) relative to the laminar solutions for different values of $\mathcal{R}$. The laminar and fully turbulent smooth solutions are also shown.
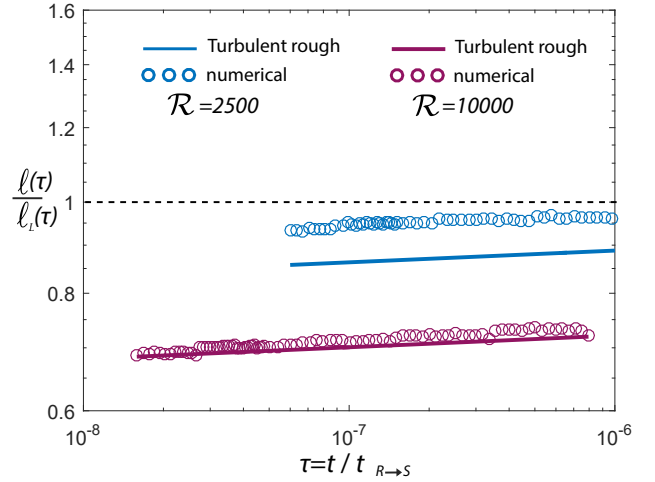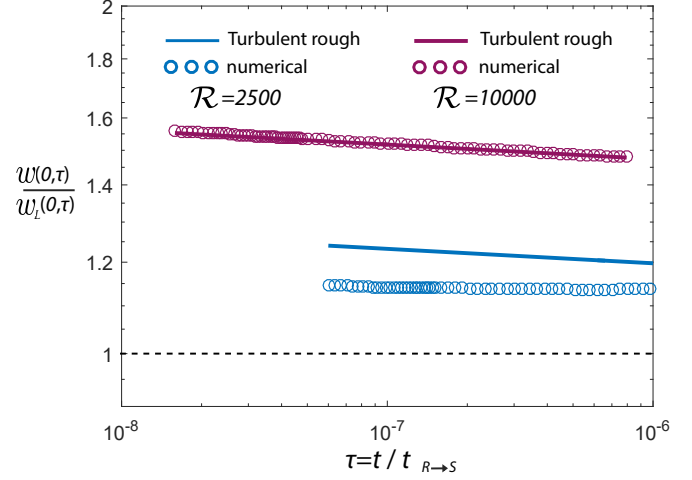


Figure 8: Laminar-Turbulent Rough case: The evolution of the fracture width (top) and fracture length (bottom) relative to the laminar solutions for two different Reynolds numbers.

relations for the evolution of friction factor with Reynolds number and roughness obtained for pipe to account for the complete transition from laminar to rough turbulent flow as function of the inlet Reynolds number for height-contained hydraulic fractures (i.e. PKN fractures). We have validated our numerical scheme on the laminar case. The scheme is also able to capture the fully turbulent solutions (fully turbulent smooth or fully turbulent rough) accurately.

For large inlet Reynolds number $\mathcal{R}$ (above the critical transition to turbulent flow), the flow transition from turbulent to laminar from the inlet to the tip of the fracture. The extent of the laminar region

close to the tip shrinks to a boundary layer as the $\mathcal{R}$ increases, reaching $10^{-2}$ for $\mathcal{R} \approx 10^4$. Our numerical solution indicates that the semi-analytical solution assuming a fully turbulent smooth regime in the fracture is valid for $\mathcal{R}$ above $5 \times 10^3$. Similarly, when the roughness is taken into account, the semi-analytical solution for fully turbulent rough flow is valid for such high Reynolds numbers.

An important point that we have not addressed in this paper is the effect of the addition of friction reducers (e.g. polymer additives) in the fracturing fluid - a typical practice in high rate water fracturing treatments. The use of friction reducer is known to drastically change the laminar-turbulent

transition and will, in turn, possibly significantly changes the propagation of hydraulic fracture predicted here. We leave the effect of friction reducer on fracture propagation to future investigations.

# References

Ames, Brandon Carter and Andrew Bunger. 2015. Role of Turbulent Flow in Generating Short Hydraulic Fractures With High Net Pressure in Slickwater Treatments. In *SPE Hydraulic Fracturing Technology Conference.* Society of Petroleum Engineers. SPE-173373-MS.

Carlson, LW and TF Irvine. 1961. "Fully developed pressure drop in triangular shaped ducts." *Journal of Heat Transfer* 83(4):441–444.

Economides, M. J. and K. G. Nolte. 2000. Reservoir Stimulation. Schlumberger John Wiley & Sons.

Goldenfeld, Nigel. 2006. "Roughness-induced critical phenomena in a turbulent flow." *Physical review letters* 96(4):044503.

Jones, OC. 1976. "An improvement in the calculation of turbulent friction in rectangular ducts." *Journal of Fluids Engineering* 98(2):173–180.

Kurganov, Alexander and Chi-Tien Lin. 2007. "On the reduction of numerical dissipation in central-upwind schemes." *Commun. Comput. Phys* 2(1):141–163.

Kurganov, Alexander and Eitan Tadmor. 2000. "New high-resolution central schemes for nonlinear conservation laws and convection–diffusion equations." *Journal of Computational Physics* 160(1):241–282.

Lamb, Horace. 1895. *Hydrodynamics.* Cambridge university press.

Nessyahu, Haim and Eitan Tadmor. 1990. "Non-oscillatory central differencing for hyperbolic conservation laws." *Journal of computational physics* 87(2):408–463.

Nikuradse, Johann. 1950. *Laws of flow in rough pipes.* National Advisory Committee for Aeronautics Washington.

Nordgren, RP. 1972. "Propagation of a vertical hydraulic fracture." *Society of Petroleum Engineers Journal* 12(04):306–314.

Sadatomi, Michio, Y Sato and S Saruwatari. 1982. "Two-phase flow in vertical noncircular channels." *International Journal of Multiphase Flow* 8(6):641–655.

Sarvaramini, Erfan and Dmitry I Garagash. 2015. "Breakdown of a Pressurized Fingerlike Crack in a Permeable Solid." *Journal of Applied Mechanics* 82(6):061006.

Sneddon, IN and HA Elliot. 1946. "The opening of a Griffith crack under internal pressure." *Quart. Appl. Math* 4(3):262–267.

Tsai, Victor C and James R Rice. 2010. "A model for turbulent hydraulic fracture and application to crack propagation at glacier beds." *Journal of Geophysical Research: Earth Surface* 115(F3).

Yang, Shu-Qing and G Dou. 2010. "Turbulent drag reduction with polymer additive in rough pipes." *Journal of Fluid Mechanics* 642:279–294.

Zia, Haseeb. 2015. A numerical model for simulating sediment routing in shallow water flow PhD thesis University of Geneva.

Zia, Haseeb and Guy Simpson. under-review. "Anti-diffusive, non-oscillatory central difference scheme (adNOC) suitable for highly nonlinear advection-dominated problems." *Journal of Computational Physics* .